Cell Reports

Convergent effects of different anesthetics on changes in phase alignment of cortical oscillations

Graphical abstract

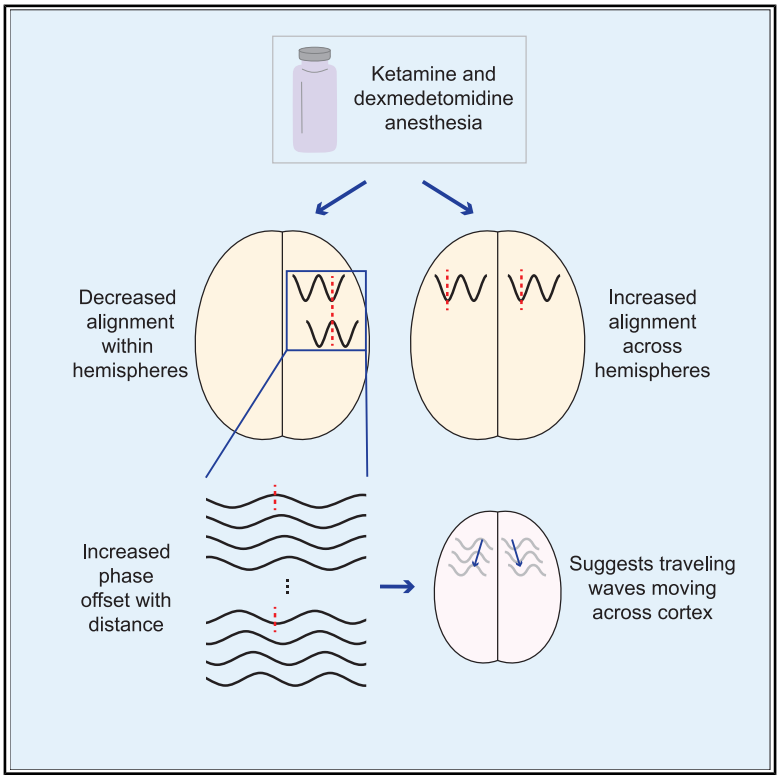

Authors

Alexandra G. Bardon, Jesus J. Ballesteros, Scott L. Brincat, ..., Yumiko Ishizawa, Emery N. Brown, Earl K. Miller

Correspondence

ekmiller@mit.edu

In brief

Bardon et al. show that different anesthetic drugs have similar effects on the phase alignment of neural oscillations across cortical areas. Neighboring regions within a hemisphere become misaligned, while homologous regions across hemispheres are more synchronized. Their results suggest a common mechanism of anesthetic-induced unconsciousness, through realignment of cortical communication.

Highlights

- Anesthetic drugs decrease alignment of oscillations in neighboring cortical areas
- These same drugs increase alignment in homologous regions across hemispheres
- Misalignment is consistent with distance-based phase offsets
- Effects are reduced with sub-anesthetic doses of drugs

Bardon et al., 2025, Cell Reports *44*, 115685
May 27, 2025
https://doi.org/10.1016/j.celrep.2025.115685

CellPress

Cell Reports

CellPress
OPEN ACCESS

Report

Convergent effects of different anesthetics on changes in phase alignment of cortical oscillations

Alexandra G. Bardon,[1] Jesus J. Ballesteros,[1,2] Scott L. Brincat,[1] Jefferson E. Roy,[1] Meredith K. Mahnke,[1] Yumiko Ishizawa,[3] Emery N. Brown,[1,3] and Earl K. Miller[1,4,*]

[1]The Picower Institute for Learning and Memory and Department of Brain and Cognitive Sciences, Massachusetts Institute of Technology, Cambridge, MA 02139, USA

[2]Department of Psychology, Ruhr-Universität-Bochum, 44801 Bochum, Germany

[3]Department of Anesthesia, Critical Care, and Pain Medicine, Massachusetts General Hospital, Harvard Medical School, Boston, MA 02139, USA

[4]Lead contact

*Correspondence: ekmiller@mit.edu

https://doi.org/10.1016/j.celrep.2025.115685

SUMMARY

Many anesthetics cause loss of consciousness despite having diverse underlying molecular and circuit actions. To explore the convergent effects of these drugs, we examine how anesthetic doses of ketamine and dexmedetomidine affect bilateral oscillations in the prefrontal cortex of nonhuman primates. Both anesthetics increase phase locking in the ventrolateral and dorsolateral prefrontal cortex, within and across hemispheres. However, the nature of the phase locking varies. Neighboring prefrontal subregions within a hemisphere show decreased phase alignment with both drugs. Local analyses within a region suggest that this finding could be explained by broad cortical distance-based effects, such as large traveling waves. In contrast, homologous areas across hemispheres become more aligned in phase. Our results suggest that both anesthetics induce strong patterns of cortical phase alignment that are markedly different from those during waking and that these patterns may be a common feature driving loss of responsiveness from different anesthetic drugs.

INTRODUCTION

Many different anesthetics exist and are widely used in medicine for similar purposes, despite having distinct mechanisms of action. The common elements by which these drugs induce similar outcomes, namely loss of consciousness (LOC), is an open question.[1,2] Their convergence is likely at a higher level, in the network dynamics driven by each drug's unique molecular effects. Previous studies have shown that various anesthetics cause an increase in delta (1–4 Hz) power[3–8] and coherence[6,7] in humans and non-human primates (NHPs). However, previous studies have not examined the phase alignment between these signals. Phase alignment may be critical in information transfer across cortex and in consciousness.[9–14] Thus, we examined whether changes in phase alignment might underlie the convergent effects (i.e., LOC) across different anesthetics.

We used ketamine and dexmedetomidine, two anesthetics with distinct molecular actions on different pathways. Ketamine is an *N*-methyl-D-aspartate (NMDA) receptor antagonist. Dexmedetomidine agonizes α2 adrenergic receptors, mainly in the locus coeruleus, which reduces norepinephrine in the cortex. At anesthetic doses, they both produce the same behavioral outcome: LOC.

We examined bilateral recordings from the prefrontal cortex (PFC) of macaques before and after administration of ketamine and dexmedetomidine. Most studies of NHPs have recorded activity from one hemisphere. Our recordings afforded us the opportunity to examine phase alignment with and between hemispheres, both in the awake state and after LOC. We quantified phase locking, a common measure of the consistency of local field potential (LFP) signals between different areas. We also examined the phase offsets at which these LFPs were locked, which gives additional insights into cortical synchrony patterns.

We found evidence that ketamine and dexmedetomidine had similar effects in how they changed phase relationships between low-frequency LFPs. The drugs increased phase locking across all recorded regions of PFC, but the nature of this phase locking was not homogeneous. Between different regions within a hemisphere, both of the drugs reduced the alignment of LFP activity. Between homologous regions across hemispheres, they caused activity to become more consistently aligned. These shifts suggest that anesthetics act through complex changes in phase alignment of oscillatory dynamics that are common across drugs despite their different molecular actions.

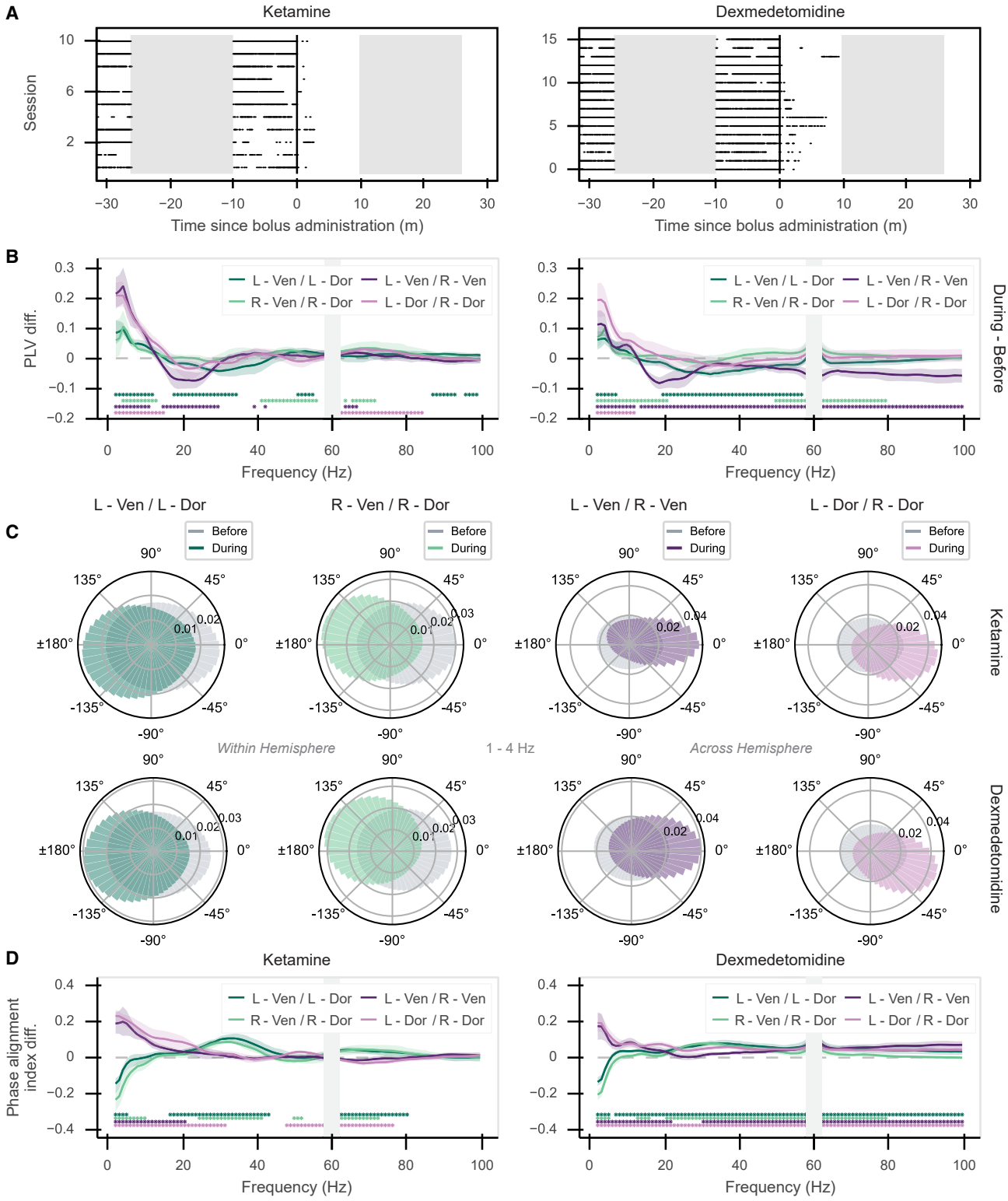

Figure 1. Anesthetics increased phase offsets within hemispheres and decreased them across hemispheres

(A) Behavioral responses to the lever-pressing task. Black dots indicate lever presses; black line at time 0 indicates drug administration. Gray areas indicate time without the lever task (further analysis focuses on data from this period).

(B) Difference (during–before anesthetics) in phase locking value (PLV).

(legend continued on next page)

RESULTS

We examined simultaneous recordings from electrode arrays in the right and left dorsolateral (R-Dor, L-Dor) and ventrolateral (R-Ven, L-Ven) PFC. A lever-pressing task, which involved pressing a lever for a reward after a tone, was used to assess loss of responsiveness as a measure of LOC. The task was conducted before, during, and after anesthetic administration, as indicated by periods with a white background in Figure 1A. Anesthetic doses of ketamine (10 mg/kg) and dexmedetomidine (20 μg/kg) caused monkeys to stop responding (dots indicate responses) shortly after their administration (vertical line at time zero), indicating the onset of anesthetic effects (Figure 1A). To minimize movement- and reward-related differences, neural data for all analyses were taken from periods without the lever task (gray boxes, Figure 1A). Animals remained unresponsive even after the lever task was reinstated at 25 min post-drug. LFPs were pre-processed using a statistically robust common average referencing technique (rCAR), which better preserves phase accuracy than other methods[15] (see LFP Processing in STAR Methods for a discussion of referencing techniques).

Ketamine and dexmedetomidine at anesthetic doses increased low-frequency LFP power (Figure S1B). Across all sessions, both drugs caused an increase in power below 16 Hz that was especially prominent in the delta (1–4 Hz) and theta (4–8 Hz) bands (Figure S1B).

Anesthetics increased LFP phase locking

Both drugs caused an increase in phase locking at low frequencies. Figure 1B shows the change in phase locking induced by each anesthetic, as measured by the phase locking value (PLV) (values before and during anesthesia shown in Figures S2B and S2C). It shows the average phase locking between LFPs from all possible pairs of electrodes in the four arrays implanted in the L-Dor, R-Dor, L-Ven, and R-Ven PFC. Here and elsewhere, comparisons within hemispheres are colored green and those across hemispheres are colored purple.

After drug delivery, there was a significant increase in average phase locking at low frequencies (1–8 Hz) between the dorsolateral and ventrolateral PFC within each hemisphere and across the two hemispheres (Figure 1B). The increase indicated that the relative phase between pairs of LFPs became more consistent. Note that this increase in phase locking did not necessarily mean the phases were aligned, a point we take up below. There was a negative change in phase locking between ventrolateral PFC in either hemisphere in the beta range (13–30 Hz), as well as in the gamma range for dexmedetomidine (60–100 Hz), due to higher PLVs in this range during waking. Additional significant changes in phase locking occurred at higher frequencies, but these effects were smaller than those seen at the low frequencies. The PLV metric is independent of power,[16–18] so the increased phase locking was not due to higher delta power during anesthesia.

We confirmed this effect using another measure of phase locking, coherence. In contrast to PLV, coherence uses both phase and power to measure how linearly predictable one signal is from another. This analysis yielded similar results: an increase in signal consistency at low frequencies (Figure S2A). There were also similar trends for the "diagonal" comparisons across both subregions and hemispheres (R-Dor vs. L-Ven and L-Dor vs. R-Ven), although these effects did not always reach significance due to increased variability (Figures S3A and S3B). While there was variation between the two monkeys, likely due to a combination of biological variation and slight differences in array placement, these effects in the low frequencies were generally directionally consistent across different monkeys and sessions (Figures S2F and S2G).

Anesthetics reduced alignment within hemispheres but increased it across hemispheres

The increase in low-frequency phase locking caused by ketamine and dexmedetomidine at anesthetic doses did not necessarily mean that the phases in all areas became more aligned. We found that the phase offsets shifted out of alignment within hemispheres while becoming more aligned across hemispheres.

Figure 1C shows the distribution of phase offsets in the 1- to 4-Hz range. The gray bars show the phase offsets before drug delivery. They were nearly uniform across hemispheres and biased toward in-phase (0° offset) within hemispheres. The colored bars show phase offsets after anesthetic administration. They indicate decreased phase alignment between ventrolateral and dorsolateral arrays (L-Ven vs. L-Dor, R-Ven vs. R-Dor; Figure 1C, green). By contrast, there was increased phase alignment across hemispheres (L-Ven vs. R-Ven, L-Dor vs. R-Dor; Figure 1C, purple).

The changes in phase offsets were mainly in the lower frequencies. To quantify this effect, we calculated a phase alignment index, measuring the average cosine of the phase offsets. Figure 1D shows the change in phase alignment index with anesthetics (values before and during anesthesia shown in Figures S2D and S2E). Anesthetic doses of both ketamine and dexmedetomidine caused a significant decrease in phase alignment within hemispheres (negative alignment index, more toward 180°) at frequencies in the 1- to 4-Hz range (Figure 1D, green lines). Across hemispheres, there was a significant increase in phase alignment (positive alignment index, more toward 0°) for the same frequency range (Figure 1D, purple lines). Ketamine also caused a significant increase in within-hemisphere phase alignment in the 20- to 40-Hz range, and both drugs had a range of small but statistically significant effects on higher-frequency phase alignment. The effects were directionally consistent across animals, sessions, and drugs (Figures S2H–S2K). Along the diagonal comparisons (L-Ven vs. R-Dor, R-Ven vs. L-Dor) we also found a slight decrease in phase-aligned signals with dexmedetomidine, but the effect was not significant with ketamine (Figures S3C and S3D). In addition, we tested the changes in phase offsets with

(C) Histogram of phase offsets between all channel pairs in indicated regions before (gray) and during (colored) anesthetics in the 1- to 4-Hz range.
(D) Phase alignment index difference (during–before anesthetics). Line plots show mean and 99% confidence intervals across sessions. Asterisks indicate significant differences before and during anesthetic effects ($p < 0.01$, corrected for multiple comparisons). Gray bar at 60 Hz due to line noise-filtering effects. See also Figures S2–S4.

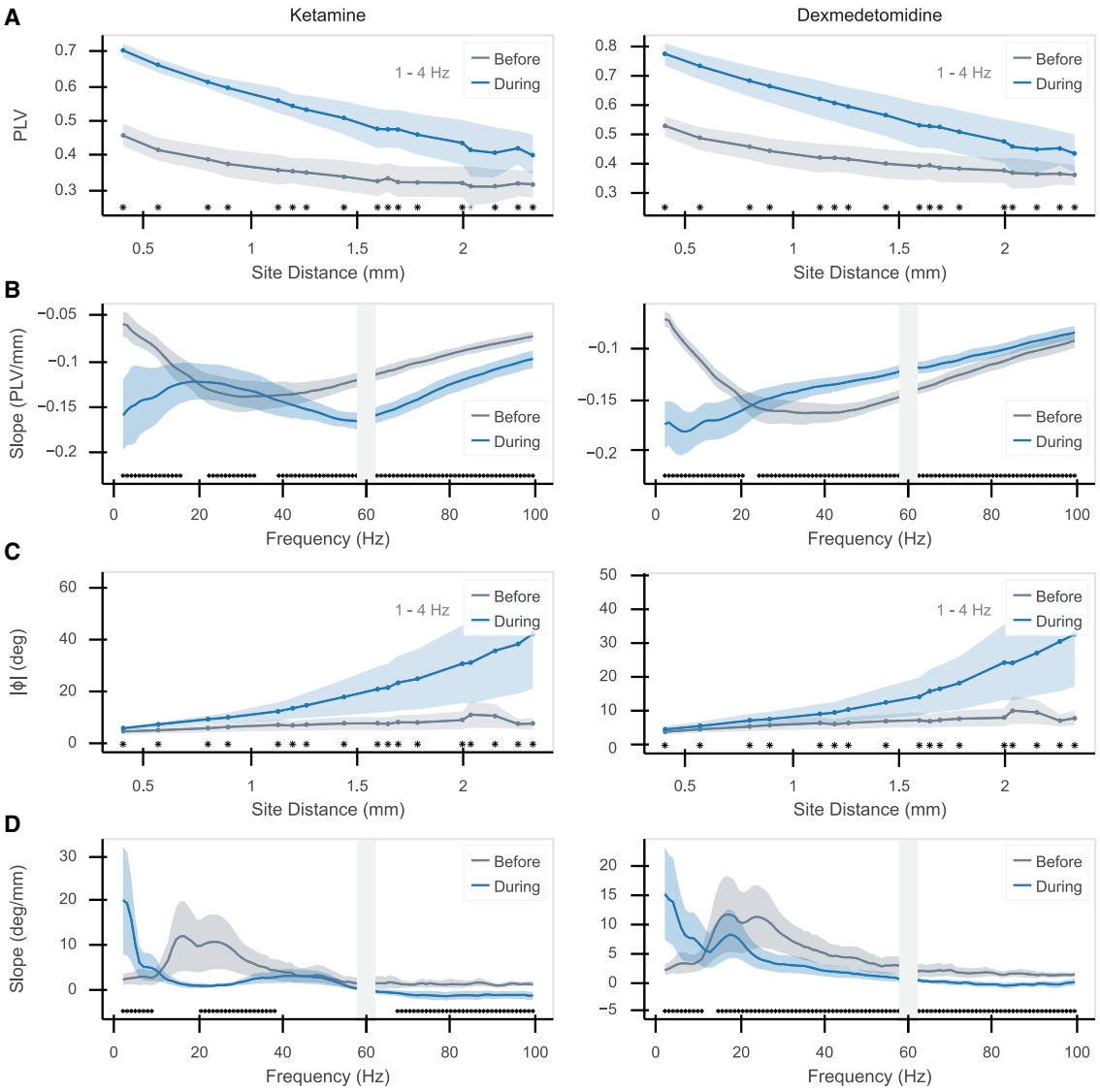

Figure 2. Phase locking weakened, and LFPs became less phase aligned with distance

(A) PLV vs. distance within an array, before (gray) and during (blue) anesthetics, in the low-frequency range (1–4 Hz).

(B) Slope of PLV vs. distance (as in A) as a function of frequency.

(C) Phase offset (absolute value) vs. distance (1–4 Hz).

(D) Slope of phase offset (absolute value) vs. distance (as in C) as a function of frequency. Line plots show mean and 99% confidence intervals across sessions. Asterisks indicate significant differences before and during anesthetic effects ($p < 0.01$, corrected for multiple comparisons). Gray bar at 60 Hz due to line noise-filtering effects.

multiple LFP referencing techniques to ensure that our findings did not rely upon the referencing scheme. In addition to the method used here, rCAR, we tested no re-referencing and global mean subtraction (see STAR Methods for further discussion of referencing). All techniques led to similar trends in changes in phase offsets with anesthetics (Figure S4).

Increased phase offset with distance was amplified by anesthetics

To explore whether the observed cross-region phase offsets could be explained by distance effects, we quantified how the phase locking and phase offsets changed with distance between electrodes within an array, where precise relative locations of recording sites were known. We found that in the awake PFC, phase locking decreased and phase offset increased slightly with distance within each recording array. These effects were stronger with anesthetics. The phase locking and phase offsets were relatively linear as a function of distance (example of low-frequency PLV in Figure 2A), so we also examined the slopes of these lines.

Before drug delivery, phase locking decreased with electrode distance within each array in the low-frequency range (1–4 Hz)

(Figure 2A). This effect existed across a wide range of frequencies (Figure 2B, decrease indicated by all negative slopes). Phase offset with distance was positive but nearly flat before drug delivery for the low frequencies (gray lines, Figure 2C). By contrast, the mid-range frequencies (15–40 Hz) showed a marked increase in phase offset with distance before drug delivery (Figure 2D), likely due to the higher activity of mid-range frequencies during waking.

Both ketamine and dexmedetomidine amplified these trends. At low frequencies, the drugs caused a sharper decline in phase locking and sharper increase in phase offset with distance (Figures 2A and 2C). Note that there are fewer pairs in an array at farther distances, which could lead to the greater variability shown, in addition to the decreased phase locking at those distances. At higher frequencies, the results were mixed. The effect of ketamine on phase locking in the gamma band (40–100 Hz) was similar to low frequencies (Figure 2B). Dexmedetomidine, by contrast, caused a flattening of the slope of PLV vs. distance between 30 and 70 Hz. Neither drug had large effects on the overall phase offsets at high frequencies (Figure 2D).

A continuation of these distance trends amplified under drug influence could explain the phase offsets between arrays in ventrolateral and dorsolateral PFC. The cortical surface distance between these arrays was ~20 mm, so given the ~20°–30° phase offset between channels at either end of the array (~2.5 mm apart), extrapolating across distance could explain the observed ~180° phase offset across regions. The phase locking at the farthest distance within an array is still above values seen between arrays, but likely levels off at longer distances.

Sub-anesthetic doses of ketamine and dexmedetomidine produced weaker effects

Sub-anesthetic doses of both drugs (1 mg/kg ketamine, 5 μg/kg dexmedetomidine) produced effects that were weak and more variable but that trended toward those seen in anesthetic doses. Sub-anesthetic ketamine caused no change in low-frequency power and a smaller increase in gamma power. For dexmedetomidine, there was a smaller increase in low-frequency power (Figure S1C). Between arrays, there were significantly smaller effects in phase locking at low frequencies compared to the higher doses of each drug (indicated by horizontal bars) with few consistent trends within or across hemispheres (indicated by asterisks) (Figure 3A). The phase offset effects were smaller under sub-anesthetic doses but often trended in the same direction (Figures 3B and 3C), and they reached significance for fewer comparisons. Within the arrays, the local distance effects were reduced. Sub-anesthetic doses caused a smaller decrease in phase locking (Figure 3D) and a smaller increase in phase offset (Figure 3E) with distance than anesthetic doses.

DISCUSSION

Ketamine and dexmedetomidine, while acting on different molecular and circuit pathways, induce similar changes in low-frequency oscillatory dynamics. These dynamics may be a marker of LOC and suggest a fundamental role for broad, low-frequency activity in driving and disrupting consciousness. We found that both anesthetics did not simply increase low-frequency cortical dynamics, they realigned them (Figure 4A). The alignment within PFC was reduced (examples highlighted in green boxes, Figure 4B), while alignment between homologous regions across hemispheres increased (purple boxes, Figure 4B). The drugs had varying effects at higher frequencies, but the low-frequency effects were the common feature between them.

The increase in low-frequency power is consistent with studies of cortical LFPs in animals and in electroencephalogram signals in humans for these drugs,[3–8] as well as propofol,[19–24] another widely studied anesthetic. We also observed increased LFP phase locking, as previously observed in various cortical regions with ketamine,[7] dexmedetomidine,[6] and propofol.[23,24] However, our study shows that underlying the phase locking is a realignment of phases, which may affect conscious function.

Within a hemisphere, the ventrolateral and dorsolateral PFC became less phase aligned at low frequencies, with phase offsets shifting away from 0°. These offsets may fragment within-hemisphere communication as periods of excitability become misaligned.[9–14,25] In fact, propofol has been shown to fragment activity and decrease information transfer across long distances (>2 cm) in the human cortex,[26–28] and to prevent sensory signals from reaching the macaque frontal cortex.[29,30] Information transfer in the cortex is also disrupted by ketamine[31] and NMDA receptor antagonism.[32] While phases were not misaligned at all times, LFPs were more often out of phase, and such ''relative coordination'' can still strongly influence network activity.[33]

In contrast to the fragmentation of activity within a hemisphere, homologous regions across hemispheres became more aligned. The increase in interhemispheric alignment of activity by anesthetics seems to reverse the pattern observed in the awake, cognitively engaged brain. In such a case, the two hemispheres can function semi-independently, at least for visual cognition.[34] During quiet wakefulness and anesthesia, however, cross-hemispheric synchrony increases in mice,[35] in line with our observations. This synchrony in mice was dependent upon the corpus callosum,[35] which preferentially connects homologous regions.[36] Such synchrony could also be partially mediated by subcortical regions like the thalamus, a potential hub of interhemispheric communication.[37,38] Experimental and modeling work show that low-frequency oscillations and thalamocortical connections may be involved in information transfer between cortical regions,[39,40] which may be disrupted during anesthesia, thus leading to unconsciousness.[29,41,42]

Our observations of low-frequency changes in LFP signals could also be explained by the activity of cortical layer 5 pyramidal neurons, which anesthetics influence.[43–47] These neurons contribute significantly to the LFP and have low pass filtering properties at their somas.[48–50] They may be involved in the increases in power and phase locking observed during anesthesia. They also play a prominent role in thalamocortical loops.[51] Thalamocortical connectivity is hypothesized to play a major role in consciousness[13,45,52–56] and in anesthetic-induced dissociation[57] or unconsciousness.[23,24,41,42,58–62] Simultaneous recordings and stimulation in the cortex and thalamus during anesthesia will clarify the role that these interactions play in driving the broad phase-offset activity observed here.

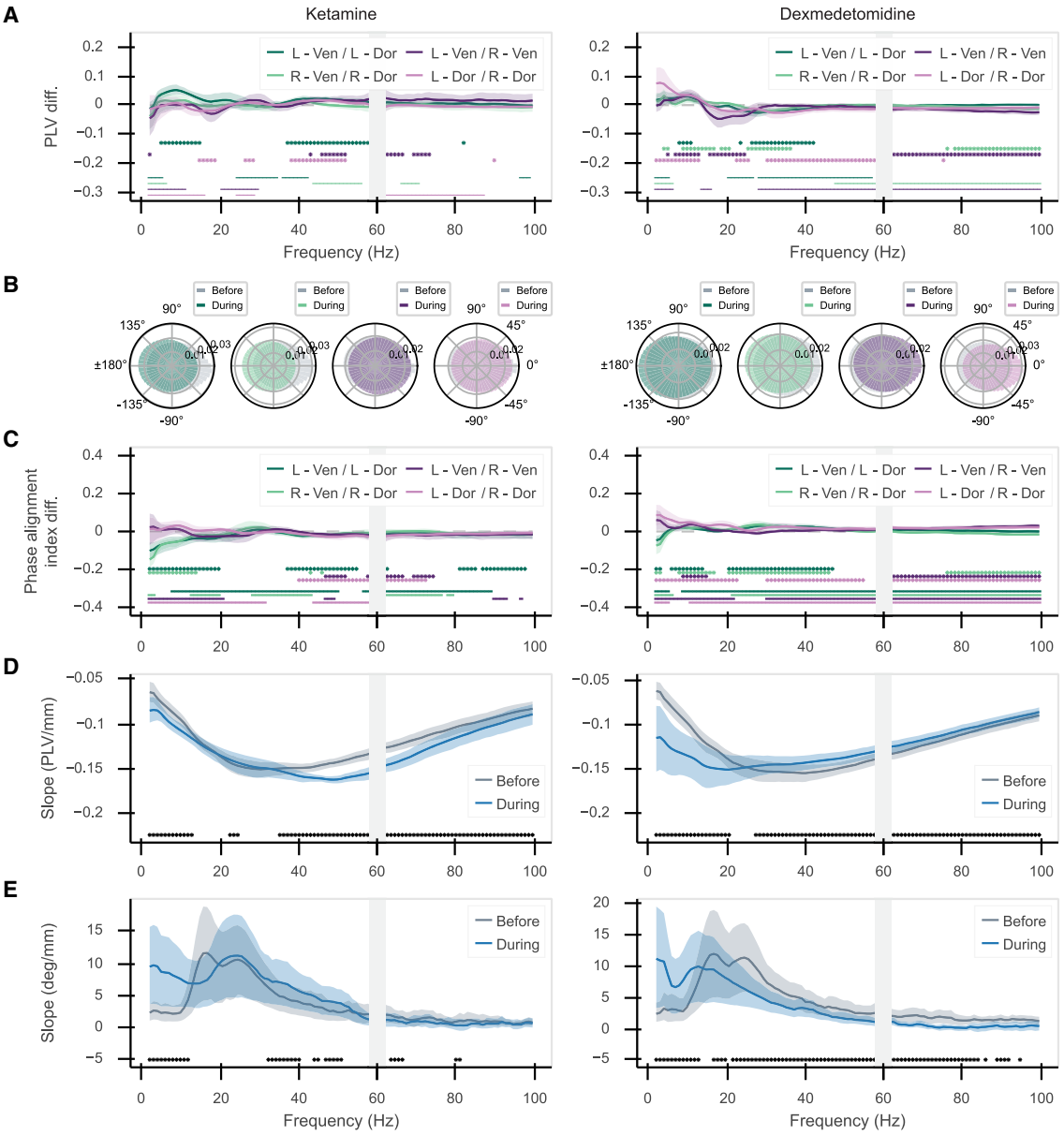

Figure 3. Sub-anesthetic doses of ketamine and dexmedetomidine produce weaker effects

(A) Change in PLV.

(B) Histograms of phase offsets.

(C) Change in phase alignment index.

(D) Phase locking slope vs. frequency within array.

(E) Phase offset (absolute value) slope vs. frequency within array. Line plots show mean and 99% confidence intervals across sessions. Asterisks indicate significant differences before and during anesthetic effects ($p < 0.01$, corrected for multiple comparisons). Gray bar at 60 Hz due to line noise-filtering effects. Horizontal bars in (A) and (C) indicate significant differences between low and high doses of anesthetics ($p < 0.01$, corrected for multiple comparisons).

The low-frequency offsets that we observed were consistent across entire arrays, suggesting the observed effects come from spatially broad oscillations. Furthermore, there was a gradient of phase offsets. Extrapolating the local phase-offset effects within an array to longer distances between arrays could explain the reduced phase alignment between the ventrolateral and dorsolateral PFC during anesthesia. In fact, this relationship suggested that these effects could be due to large traveling waves that move between the areas; Figure 4C shows an example from our recordings of such a wave traveling across a single electrode array with anesthesia. Large-scale cortical traveling waves are known to occur spontaneously during anesthesia.[63–65] These waves may play an essential role in shaping neural activity when awake[66–70] and severely limiting it during anesthesia.[65,71]

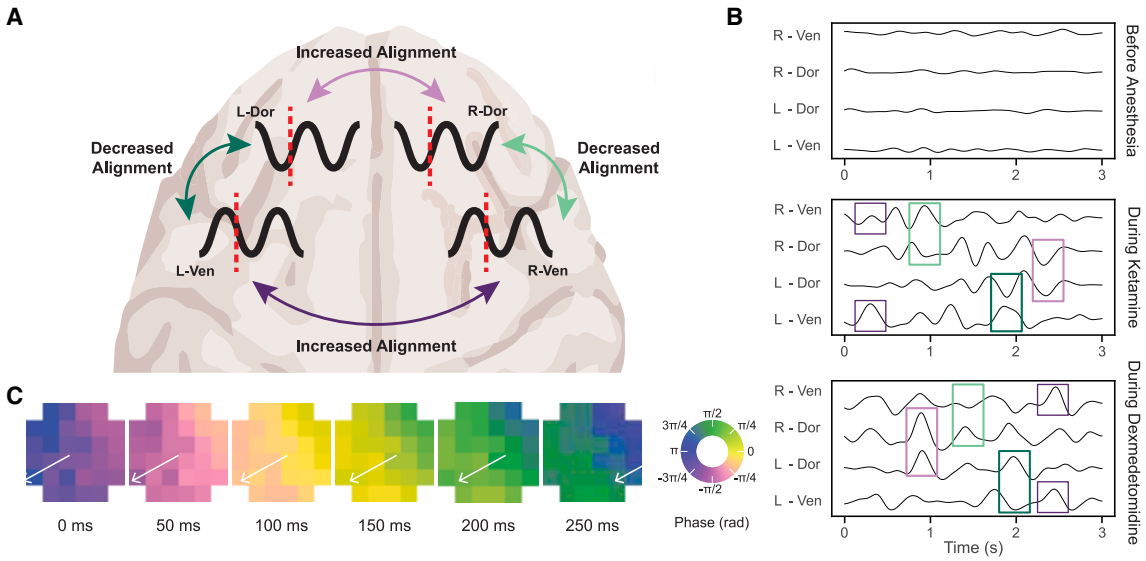

Figure 4. Anesthetics fragment cortical activity within a hemisphere but synchronize it across hemispheres

(A) Ketamine and dexmedetomidine both cause phases of low-frequency oscillatory activity to become less aligned between different regions of PFC and more aligned between homologous regions across hemispheres.

(B) Sample delta (1–4 Hz) range filtered LFP signals before anesthesia (top), with ketamine (middle), and with dexmedetomidine (bottom). Raw LFP traces shown in Figure S1A. Purple boxes show examples of increased across-hemisphere phase alignment, and green boxes show examples of decreased within-hemisphere phase alignment.

(C) Example of a traveling wave. Phase of low-frequency (1–4 Hz) LFP signal in an electrode array across time from a recording with ketamine. Each square represents one electrode contact, colored according to its instantaneous phase at the indicated time.

Limitations of the study

We observed changes in oscillatory alignment during different types of anesthesia, with the strength of phase alignment correlating with anesthetic dose. However, we did not establish a causal link between these oscillations and LOC. Further research is needed to uncover causal mechanisms. More anesthetics will need to be tested before we can conclude that similar effects underlie all LOC due to anesthesia.

Conclusion

Our results suggest that LOC from anesthetic doses of ketamine and dexmedetomidine is associated with changes in the alignment of low-frequency signals within and between cerebral hemispheres. These effects were severely weakened by sub-anesthetic doses insufficient to cause loss of responsiveness. Despite their different molecular-level mechanisms, we found similar network-level effects between the two drugs. Thus, cortical network-level activity may be the optimal viewpoint for understanding the convergent mechanisms of different anesthetics. General anesthesia can exacerbate disorders such as dementia, anxiety, depression, attention-deficit/hyperactivity disorder, and bipolar disorder, especially in children, the elderly, and vulnerable populations.[72–76] It can also interact dangerously with medications that treat mental illness.[77] Current anesthesia monitoring focuses on vital signs rather than brain activity,[78] risking overmedication and thus increased incidence of these disorders. Identifying common neural signatures of unconsciousness will improve real-time monitoring in medical practice, enabling precise anesthetic dosing and reducing risk for a broad population.[78,79]

RESOURCE AVAILABILITY

Lead contact

Requests for further information and resources should be directed to and will be fulfilled by the lead contact, Earl K. Miller (ekmiller@mit.edu).

Materials availability

This study did not generate new unique reagents.

Data and code availability

- The electrophysiology data reported in this paper will be shared by the lead contact upon request.
- This paper does not report original code.
- Any additional information required to reanalyze the data reported in this paper is available from the lead contact upon request.

ACKNOWLEDGMENTS

The authors thank Sebastian Gallo and the MIT Division of Comparative Medicine for assistance with NHPs. The authors acknowledge the MIT Office of Research Computing and Data for providing high-performance computing resources that have contributed to the research results reported within this paper. This material is based upon work supported by the US Department of Energy, Office of Science, Office of Advanced Scientific Computing Research, under award no. DE-SC0024386 (A.G.B.). This work was funded by National Institute of Mental Health (NIMH) 1R01MH131715-01 (E.K.M.), NIMH R01MH11559 (E.K.M.), NIH 1R21AG077275-01A1 (Y.I.), The Simons Center for the Social Brain (E.K.M.), The Freedom Together Foundation (E.N.B. and E.K.M.), and The Picower Institute for Learning and Memory (E.N.B. and E.K.M.). This report was prepared as an account of work sponsored by an agency of the US government. Neither the US government nor any agency thereof, nor any of their employees, makes any warranty, express or implied, or assumes any legal liability or responsibility for the accuracy, completeness, or

usefulness of any information, apparatus, product, or process disclosed, or represents that its use would not infringe privately owned rights. Reference herein to any specific commercial product, process, or service by trade name, trademark, manufacturer, or otherwise does not necessarily constitute or imply its endorsement, recommendation, or favoring by the US government or any agency thereof. The views and opinions of authors expressed herein do not necessarily state or reflect those of the US government or any agency thereof.

AUTHOR CONTRIBUTIONS

Conceptualization, A.G.B., J.J.B., S.L.B., Y.I., E.N.B., and E.K.M. Investigation J.J.B., J.E.R., and M.K.M. Data curation, J.J.B. and S.L.B. Formal analysis, A. G.B., S.L.B., and E.K.M. Supervision, Y.I., E.N.B., and E.K.M. Writing – original draft, A.G.B. and E.K.M. Writing – review & editing, A.G.B., J.J.B., S.L.B., and E.K.M. Funding acquisition, Y.I., E.N.B., and E.K.M.

DECLARATION OF INTERESTS

E.N.B. holds patents on anesthetic state monitoring and control; holds founding interest in PASCALL, a start-up developing physiological monitoring systems; and receives royalties from intellectual property through Massachusetts General Hospital licensed to Masimo. The interests of E.N.B. were reviewed and are managed by Massachusetts General Hospital and Mass General Brigham in accordance with their conflict of interest policies.

STAR★METHODS

Detailed methods are provided in the online version of this paper and include the following:

- KEY RESOURCES TABLE
- EXPERIMENTAL MODEL AND STUDY PARTICIPANT DETAILS
  - Experimental design
- METHOD DETAILS
  - LFP processing
  - Spectral analysis
  - PLV, coherence, phase offset
  - Phase histograms
  - Instantaneous phase
- QUANTIFICATION AND STATISTICAL ANALYSIS

SUPPLEMENTAL INFORMATION

Supplemental information can be found online at https://doi.org/10.1016/j.celrep.2025.115685.

Received: March 25, 2024
Revised: March 15, 2025
Accepted: April 18, 2025
Published: May 9, 2025

REFERENCES

1. Brown, E.N., Purdon, P.L., and Van Dort, C.J. (2011). General Anesthesia and Altered States of Arousal: A Systems Neuroscience Analysis. Annu. Rev. Neurosci. *34*, 601–628. https://doi.org/10.1146/annurev-neuro-060909-153200.
2. Bonhomme, V., Staquet, C., Montupil, J., Defresne, A., Kirsch, M., Martial, C., Vanhaudenhuyse, A., Chatelle, C., Larroque, S.K., Raimondo, F., et al. (2019). General Anesthesia: A Probe to Explore Consciousness. Front. Syst. Neurosci. *13*, 36. https://doi.org/10.3389/fnsys.2019.00036.
3. Purdon, P.L., Sampson, A., Pavone, K.J., and Brown, E.N. (2015). Clinical Electroencephalography for Anesthesiologists. Anesthesiology *123*, 937–960. https://doi.org/10.1097/ALN.0000000000000841.
4. Akeju, O., Song, A.H., Hamilos, A.E., Pavone, K.J., Flores, F.J., Brown, E. N., and Purdon, P.L. (2016). Electroencephalogram signatures of ketamine anesthesia-induced unconsciousness. Clin. Neurophysiol. *127*, 2414–2422. https://doi.org/10.1016/j.clinph.2016.03.005.
5. Vlisides, P.E., Bel-Bahar, T., Lee, U., Li, D., Kim, H., Janke, E., Tarnal, V., Pichurko, A.B., McKinney, A.M., Kunkler, B.S., et al. (2017). Neurophysiologic Correlates of Ketamine Sedation and Anesthesia. Anesthesiology *127*, 58–69. https://doi.org/10.1097/ALN.0000000000001671.
6. Ballesteros, J.J., Briscoe, J.B., and Ishizawa, Y. (2020). Neural signatures of α2-Adrenergic agonist-induced unconsciousness and awakening by antagonist. Elife *9*, e57670. https://doi.org/10.7554/eLife.57670.
7. Ballesteros, J.J., Huang, P., Patel, S.R., Eskandar, E.N., and Ishizawa, Y. (2020). Dynamics of Ketamine-induced Loss and Return of Consciousness across Primate Neocortex. Anesthesiology *132*, 750–762. https://doi.org/10.1097/ALN.0000000000003159.
8. Garwood, I.C., Chakravarty, S., Donoghue, J., Mahnke, M., Kahali, P., Chamadia, S., Akeju, O., Miller, E.K., and Brown, E.N. (2021). A hidden Markov model reliably characterizes ketamine-induced spectral dynamics in macaque local field potentials and human electroencephalograms. PLoS Comput. Biol. *17*, e1009280. https://doi.org/10.1371/journal.pcbi.1009280.
9. Aertsen, A.M., Gerstein, G.L., Habib, M.K., and Palm, G. (1989). Dynamics of neuronal firing correlation: modulation of "effective connectivity." J. Neurophysiol. *61*, 900–917. https://doi.org/10.1152/jn.1989.61.5.900.
10. Varela, F., Lachaux, J.-P., Rodriguez, E., and Martinerie, J. (2001). The brainweb: Phase synchronization and large-scale integration. Nat. Rev. Neurosci. *2*, 229–239. https://doi.org/10.1038/35067550.
11. Womelsdorf, T., Schoffelen, J.-M., Oostenveld, R., Singer, W., Desimone, R., Engel, A.K., and Fries, P. (2007). Modulation of Neuronal Interactions Through Neuronal Synchronization. Science *316*, 1609–1612. https://doi.org/10.1126/science.1139597.
12. Fries, P. (2015). Rhythms for Cognition: Communication through Coherence. Neuron *88*, 220–235. https://doi.org/10.1016/j.neuron.2015.09.034.
13. Modolo, J., Hassan, M., Wendling, F., and Benquet, P. (2020). Decoding the circuitry of consciousness: From local microcircuits to brain-scale networks. Net. Neurosci. *4*, 315–337. https://doi.org/10.1162/netn_a_00119.
14. Singer, W. (2018). Neuronal oscillations: unavoidable and useful? Eur. J. Neurosci. *48*, 2389–2398. https://doi.org/10.1111/ejn.13796.
15. Lepage, K.Q., Kramer, M.A., and Chu, C.J. (2014). A statistically robust EEG re-referencing procedure to mitigate reference effect. J. Neurosci. Methods *235*, 101–116. https://doi.org/10.1016/j.jneumeth.2014.05.008.
16. Lachaux, J.-P., Rodriguez, E., Martinerie, J., and Varela, F.J. (1999). Measuring phase synchrony in brain signals. Hum. Brain Mapp. *8*, 194–208. https://doi.org/10.1002/(SICI)1097-0193(1999)8:4<194::AID-HBM4>3.0.CO;2-C.
17. Srinath, R., and Ray, S. (2014). Effect of amplitude correlations on coherence in the local field potential. J. Neurophysiol. *112*, 741–751. https://doi.org/10.1152/jn.00851.2013.
18. Lepage, K.Q., and Vijayan, S. (2017). The relationship between coherence and the phase-locking value. J. Theor. Biol. *435*, 106–109. https://doi.org/10.1016/j.jtbi.2017.08.029.
19. Purdon, P.L., Pierce, E.T., Mukamel, E.A., Prerau, M.J., Walsh, J.L., Wong, K.F.K., Salazar-Gomez, A.F., Harrell, P.G., Sampson, A.L., Cimenser, A., et al. (2013). Electroencephalogram signatures of loss and recovery of consciousness from propofol. Proc. Natl. Acad. Sci. USA *110*, E1142–E1151. https://doi.org/10.1073/pnas.1221180110.
20. Akeju, O., Westover, M.B., Pavone, K.J., Sampson, A.L., Hartnack, K.E., Brown, E.N., and Purdon, P.L. (2014). Effects of Sevoflurane and Propofol on Frontal Electroencephalogram Power and Coherence. Anesthesiology *121*, 990–998. https://doi.org/10.1097/ALN.0000000000000436.
21. Mukamel, E.A., Pirondini, E., Babadi, B., Wong, K.F.K., Pierce, E.T., Harrell, P.G., Walsh, J.L., Salazar-Gomez, A.F., Cash, S.S., Eskandar, E.N., et al. (2014). A Transition in Brain State during Propofol-Induced

Unconsciousness. J. Neurosci. *34*, 839–845. https://doi.org/10.1523/JNEUROSCI.5813-12.2014.

22. Ishizawa, Y., Ahmed, O.J., Patel, S.R., Gale, J.T., Sierra-Mercado, D., Brown, E.N., and Eskandar, E.N. (2016). Dynamics of Propofol-Induced Loss of Consciousness Across Primate Neocortex. J. Neurosci. *36*, 7718–7726. https://doi.org/10.1523/JNEUROSCI.4577-15.2016.

23. Redinbaugh, M.J., Phillips, J.M., Kambi, N.A., Mohanta, S., Andryk, S., Dooley, G.L., Afrasiabi, M., Raz, A., and Saalmann, Y.B. (2020). Thalamus Modulates Consciousness via Layer-Specific Control of Cortex. Neuron *106*, 66–75.e12. https://doi.org/10.1016/j.neuron.2020.01.005.

24. Bastos, A.M., Donoghue, J.A., Brincat, S.L., Mahnke, M., Yanar, J., Correa, J., Waite, A.S., Lundqvist, M., Roy, J., Brown, E.N., et al. (2021). Neural effects of propofol-induced unconsciousness and its reversal using thalamic stimulation. Elife *10*, e60824. https://doi.org/10.7554/eLife.60824.

25. Blackman, R.K., Crowe, D.A., DeNicola, A.L., Sakellaridi, S., Westerberg, J.A., Huynh, A.M., MacDonald, A.W., Sponheim, S.R., and Chafee, M.V. (2023). Shared Neural Activity But Distinct Neural Dynamics for Cognitive Control in Monkey Prefrontal and Parietal Cortex. J. Neurosci. *43*, 2767–2781. https://doi.org/10.1523/JNEUROSCI.1641-22.2023.

26. Lewis, L.D., Weiner, V.S., Mukamel, E.A., Donoghue, J.A., Eskandar, E.N., Madsen, J.R., Anderson, W.S., Hochberg, L.R., Cash, S.S., Brown, E.N., et al. (2012). Rapid fragmentation of neuronal networks at the onset of propofol-induced unconsciousness. Proc. Natl. Acad. Sci. USA *109*, E3377–E3386. https://doi.org/10.1073/pnas.1210907109.

27. Liang, Z., Cheng, L., Shao, S., Jin, X., Yu, T., Sleigh, J.W., and Li, X. (2020). Information Integration and Mesoscopic Cortical Connectivity during Propofol Anesthesia. Anesthesiology *132*, 504–524. https://doi.org/10.1097/ALN.0000000000003015.

28. Zelmann, R., Paulk, A.C., Tian, F., Balanza Villegas, G.A., Dezha Peralta, J., Crocker, B., Cosgrove, G.R., Richardson, R.M., Williams, Z.M., Dougherty, D.D., et al. (2023). Differential cortical network engagement during states of un/consciousness in humans. Neuron *111*, 3479–3495.e6. https://doi.org/10.1016/j.neuron.2023.08.007.

29. Tauber, J.M., Brincat, S.L., Stephen, E.P., Donoghue, J.A., Kozachkov, L., Brown, E.N., and Miller, E.K. (2023). Propofol-mediated Unconsciousness Disrupts Progression of Sensory Signals through the Cortical Hierarchy. J. Cognit. Neurosci. *36*, 1–20. https://doi.org/10.1162/jocn_a_02081.

30. Xiong, Y.(S.), Donoghue, J.A., Lundqvist, M., Mahnke, M., Major, A.J., Brown, E.N., Miller, E.K., and Bastos, A.M. (2024). Propofol-mediated loss of consciousness disrupts predictive routing and local field phase modulation of neural activity. Proc. Natl. Acad. Sci. USA *121*, e2315160121. https://doi.org/10.1073/pnas.2315160121.

31. Schroeder, K.E., Irwin, Z.T., Gaidica, M., Bentley, J.N., Patil, P.G., Mashour, G.A., and Chestek, C.A. (2016). Disruption of corticocortical information transfer during ketamine anesthesia in the primate brain. Neuroimage *134*, 459–465. https://doi.org/10.1016/j.neuroimage.2016.04.039.

32. Zick, J.L., Blackman, R.K., Crowe, D.A., Amirikian, B., DeNicola, A.L., Netoff, T.I., and Chafee, M.V. (2018). Blocking NMDAR Disrupts Spike Timing and Decouples Monkey Prefrontal Circuits: Implications for Activity-Dependent Disconnection in Schizophrenia. Neuron *98*, 1243–1255.e5. https://doi.org/10.1016/j.neuron.2018.05.010.

33. Bressler, S.L., and Kelso, J.A.S. (2001). Cortical coordination dynamics and cognition. Trends Cognit. Sci. *5*, 26–36. https://doi.org/10.1016/S1364-6613(00)01564-3.

34. Buschman, T.J., Siegel, M., Roy, J.E., and Miller, E.K. (2011). Neural substrates of cognitive capacity limitations. Proc. Natl. Acad. Sci. USA *108*, 11252–11255. https://doi.org/10.1073/pnas.1104666108.

35. Mohajerani, M.H., McVea, D.A., Fingas, M., and Murphy, T.H. (2010). Mirrored Bilateral Slow-Wave Cortical Activity within Local Circuits Revealed by Fast Bihemispheric Voltage-Sensitive Dye Imaging in Anesthetized and Awake Mice. J. Neurosci. *30*, 3745–3751. https://doi.org/10.1523/JNEUROSCI.6437-09.2010.

36. Shen, K., Mišić, B., Cipollini, B.N., Bezgin, G., Buschkuehl, M., Hutchison, R.M., Jaeggi, S.M., Kross, E., Peltier, S.J., Everling, S., et al. (2015). Stable long-range interhemispheric coordination is supported by direct anatomical projections. Proc. Natl. Acad. Sci. USA *112*, 6473–6478. https://doi.org/10.1073/pnas.1503436112.

37. Szczupak, D., Schaeffer, D.J., Tian, X., Choi, S.-H., Fang-Cheng, Iack, P. M., Campos, V.P., Mayo, J.P., Patsch, J., Mitter, C., et al. (2023). Direct interhemispheric cortical communication via thalamic commissures: a new white matter pathway in the primate brain. Cerebr. Cortex *34*, bhad394. https://doi.org/10.1093/cercor/bhad394.

38. Szczupak, D., Iack, P.M., Liu, C., IRC5, C., Tovar-Moll, F., Lent, R., and Silva, A.C. (2021). Direct Interhemispheric Cortical Communication via Thalamic Commissures: A New White-Matter Pathway in the Rodent Brain. Cerebr. Cortex *31*, 4642–4651. https://doi.org/10.1093/cercor/bhab112.

39. Saalmann, Y.B., Pinsk, M.A., Wang, L., Li, X., and Kastner, S. (2012). The Pulvinar Regulates Information Transmission Between Cortical Areas Based on Attention Demands. Science *337*, 753–756. https://doi.org/10.1126/science.1223082.

40. Saalmann, Y.B. (2014). Intralaminar and medial thalamic influence on cortical synchrony, information transmission and cognition. Front. Syst. Neurosci. *8*, 83. https://doi.org/10.3389/fnsys.2014.00083.

41. Müller, E.J., Munn, B.R., Redinbaugh, M.J., Lizier, J., Breakspear, M., Saalmann, Y.B., and Shine, J.M. (2023). The non-specific matrix thalamus facilitates the cortical information processing modes relevant for conscious awareness. Cell Rep. *42*, 112844. https://doi.org/10.1016/j.celrep.2023.112844.

42. Munn, B.R., Müller, E.J., Aru, J., Whyte, C.J., Gidon, A., Larkum, M.E., and Shine, J.M. (2023). A thalamocortical substrate for integrated information via critical synchronous bursting. Proc. Natl. Acad. Sci. USA *120*, e2308670120. https://doi.org/10.1073/pnas.2308670120.

43. LaBerge, D. (2006). Apical dendrite activity in cognition and consciousness. Conscious. Cognit. *15*, 235–257. https://doi.org/10.1016/j.concog.2005.09.007.

44. Meyer, K. (2015). The Role of Dendritic Signaling in the Anesthetic Suppression of Consciousness. Anesthesiology *122*, 1415–1431. https://doi.org/10.1097/ALN.0000000000000673.

45. Aru, J., Suzuki, M., Rutiku, R., Larkum, M.E., and Bachmann, T. (2019). Coupling the State and Contents of Consciousness. Front. Syst. Neurosci. *13*, 43. https://doi.org/10.3389/fnsys.2019.00043.

46. Aru, J., Suzuki, M., and Larkum, M.E. (2020). Cellular Mechanisms of Conscious Processing. Trends Cognit. Sci. *24*, 814–825. https://doi.org/10.1016/j.tics.2020.07.006.

47. Suzuki, M., and Larkum, M.E. (2020). General Anesthesia Decouples Cortical Pyramidal Neurons. Cell *180*, 666–676.e13. https://doi.org/10.1016/j.cell.2020.01.024.

48. London, M., and Häusser, M. (2005). Dendritic Computation. Annu. Rev. Neurosci. *28*, 503–532. https://doi.org/10.1146/annurev.neuro.28.061604.135703.

49. Lindén, H., Pettersen, K.H., and Einevoll, G.T. (2010). Intrinsic dendritic filtering gives low-pass power spectra of local field potentials. J. Comput. Neurosci. *29*, 423–444. https://doi.org/10.1007/s10827-010-0245-4.

50. Buzsáki, G., Anastassiou, C.A., and Koch, C. (2012). The origin of extracellular fields and currents — EEG, ECoG, LFP and spikes. Nat. Rev. Neurosci. *13*, 407–420. https://doi.org/10.1038/nrn3241.

51. Mease, R.A., and Gonzalez, A.J. (2021). Corticothalamic Pathways From Layer 5: Emerging Roles in Computation and Pathology. Front. Neural Circuits *15*, 730211. https://doi.org/10.3389/fncir.2021.730211.

52. Shumikhina, S., and Molotchnikoff, S. (1999). Pulvinar participates in synchronizing neural assemblies in the visual cortex, in cats. Neurosci. Lett. *272*, 135–139. https://doi.org/10.1016/S0304-3940(99)00497-8.

53. Jones, E.G. (2001). The thalamic matrix and thalamocortical synchrony. Trends Neurosci. *24*, 595–601. https://doi.org/10.1016/S0166-2236(00)01922-6.

54. Mitchell, A.S., and Chakraborty, S. (2013). What does the mediodorsal thalamus do? Front. Syst. Neurosci. *7*, 37. https://doi.org/10.3389/fnsys.2013.00037.

55. Sherman, S.M. (2017). Functioning of Circuits Connecting Thalamus and Cortex. In Comprehensive Physiology, Y.S. Prakash, ed. (Wiley), pp. 713–739. https://doi.org/10.1002/cphy.c160032.

56. Eradath, M.K., Pinsk, M.A., and Kastner, S. (2021). A causal role for the pulvinar in coordinating task-independent cortico–cortical interactions. J. Comp. Neurol. *529*, 3772–3784. https://doi.org/10.1002/cne.25193.

57. Vesuna, S., Kauvar, I.V., Richman, E., Gore, F., Oskotsky, T., Sava-Segal, C., Luo, L., Malenka, R.C., Henderson, J.M., Nuyujukian, P., et al. (2020). Deep posteromedial cortical rhythm in dissociation. Nature *586*, 87–94. https://doi.org/10.1038/s41586-020-2731-9.

58. Ching, S., Cimenser, A., Purdon, P.L., Brown, E.N., and Kopell, N.J. (2010). Thalamocortical model for a propofol-induced α-rhythm associated with loss of consciousness. Proc. Natl. Acad. Sci. USA *107*, 22665–22670. https://doi.org/10.1073/pnas.1017069108.

59. Flores, F.J., Hartnack, K.E., Fath, A.B., Kim, S.-E., Wilson, M.A., Brown, E.N., and Purdon, P.L. (2017). Thalamocortical synchronization during induction and emergence from propofol-induced unconsciousness. Proc. Natl. Acad. Sci. USA *114*, E6660–E6668. https://doi.org/10.1073/pnas.1700148114.

60. Hutt, A., Lefebvre, J., Hight, D., and Sleigh, J. (2018). Suppression of underlying neuronal fluctuations mediates EEG slowing during general anaesthesia. Neuroimage *179*, 414–428. https://doi.org/10.1016/j.neuroimage.2018.06.043.

61. Malekmohammadi, M., Price, C.M., Hudson, A.E., DiCesare, J.A.T., and Pouratian, N. (2019). Propofol-induced loss of consciousness is associated with a decrease in thalamocortical connectivity in humans. Brain *142*, 2288–2302. https://doi.org/10.1093/brain/awz169.

62. Tasserie, J., Uhrig, L., Sitt, J.D., Manasova, D., Dupont, M., Dehaene, S., and Jarraya, B. (2022). Deep brain stimulation of the thalamus restores signatures of consciousness in a nonhuman primate model. Sci. Adv. *8*, eabl5547. https://doi.org/10.1126/sciadv.abl5547.

63. Roland, P.E., Hanazawa, A., Undeman, C., Eriksson, D., Tompa, T., Nakamura, H., Valentiniene, S., and Ahmed, B. (2006). Cortical feedback depolarization waves: A mechanism of top-down influence on early visual areas. Proc. Natl. Acad. Sci. USA *103*, 12586–12591. https://doi.org/10.1073/pnas.0604925103.

64. Townsend, R.G., Solomon, S.S., Chen, S.C., Pietersen, A.N.J., Martin, P.R., Solomon, S.G., and Gong, P. (2015). Emergence of Complex Wave Patterns in Primate Cerebral Cortex. J. Neurosci. *35*, 4657–4662. https://doi.org/10.1523/JNEUROSCI.4509-14.2015.

65. Bhattacharya, S., Donoghue, J.A., Mahnke, M., Brincat, S.L., Brown, E.N., and Miller, E.K. (2022). Propofol Anesthesia Alters Cortical Traveling Waves. J. Cognit. Neurosci. *34*, 1274–1286. https://doi.org/10.1162/jocn_a_01856.

66. Helfrich, R.F., Fiebelkorn, I.C., Szczepanski, S.M., Lin, J.J., Parvizi, J., Knight, R.T., and Kastner, S. (2018). Neural Mechanisms of Sustained Attention Are Rhythmic. Neuron *99*, 854–865.e5. https://doi.org/10.1016/j.neuron.2018.07.032.

67. Muller, L., Chavane, F., Reynolds, J., and Sejnowski, T.J. (2018). Cortical travelling waves: mechanisms and computational principles. Nat. Rev. Neurosci. *19*, 255–268. https://doi.org/10.1038/nrn.2018.20.

68. Alexander, D.M., Ball, T., Schulze-Bonhage, A., and Van Leeuwen, C. (2019). Large-scale cortical travelling waves predict localized future cortical signals. PLoS Comput. Biol. *15*, e1007316. https://doi.org/10.1371/journal.pcbi.1007316.

69. Davis, Z.W., Muller, L., Martinez-Trujillo, J., Sejnowski, T., and Reynolds, J.H. (2020). Spontaneous travelling cortical waves gate perception in behaving primates. Nature *587*, 432–436. https://doi.org/10.1038/s41586-020-2802-y.

70. Effenberger, F., Carvalho, P., Dubinin, I., and Singer, W. (2022). The functional role of oscillatory dynamics in neocortical circuits: a computational perspective. Proc. Natl. Acad. Sci. USA *122*, e2412830122. https://doi.org/10.1073/pnas.2412830122.

71. Chamadia, S., Pedemonte, J.C., Hahm, E.Y., Mekonnen, J., Ibala, R., Gitlin, J., Ethridge, B.R., Qu, J., Vazquez, R., Rhee, J., et al. (2019). Delta oscillations phase limit neural activity during sevoflurane anesthesia. Commun. Biol. *2*, 415. https://doi.org/10.1038/s42003-019-0664-3.

72. Sun, M., Chen, W.-M., Wu, S.-Y., and Zhang, J. (2024). Risk of Pediatric Bipolar Disorder After General Anesthesia in Infants and Toddlers: A Propensity Score-Matched Population-Based Cohort Study. Schizophr. Bull. *50*, 784–791. https://doi.org/10.1093/schbul/sbae053.

73. Song, J.Y., Cha, H.R., Lee, S.W., Ha, E.K., Kim, J.H., and Han, M.Y. (2023). Association Between Receipt of General Anesthesia During Childhood and Attention Deficit Hyperactive Disorder and Neurodevelopment. J. Korean Med. Sci. *38*, e42. https://doi.org/10.3346/jkms.2023.38.e42.

74. Bakri, M., Ismail, E., Ali, M., Elsedfy, G., Sayed, T., and Ibrahim, A. (2015). Behavioral and emotional effects of repeated general anesthesia in young children. Saudi J. Anaesth. *9*, 161. https://doi.org/10.4103/1658-354X.152843.

75. Chen, C., Lin, C., Chen, K., Kuo, Y., Li, C., and Chung, C. (2014). Increased risk of dementia in people with previous exposure to general anesthesia: A nationwide population-based case–control study. Alzheimer's Dementia *10*, 196–204. https://doi.org/10.1016/j.jalz.2013.05.1766.

76. Bratzke, L.C., Koscik, R.L., Schenning, K.J., Clark, L.R., Sager, M.A., Johnson, S.C., Hermann, B.P., and Hogan, K.J. (2018). Cognitive decline in the middle-aged after surgery and anaesthesia: results from the Wisconsin Registry for Alzheimer's Prevention cohort. Anaesthesia *73*, 549–555. https://doi.org/10.1111/anae.14216.

77. Harbell, M.W., Dumitrascu, C., Bettini, L., Yu, S., Thiele, C.M., and Koyyalamudi, V. (2021). Anesthetic Considerations for Patients on Psychotropic Drug Therapies. Neurol. Int. *13*, 640–658. https://doi.org/10.3390/neurolint13040062.

78. Jung, C., Hinken, L., Fischer-Kumbruch, M., Trübenbach, D., Fielbrand, R., Schenk, I., Diegmann, O., Krauß, T., Scheinichen, D., and Schultz, B. (2021). Intraoperative monitoring parameters and postoperative delirium: Results of a prospective cross-sectional trial. Medicine *100*, e24160. https://doi.org/10.1097/MD.0000000000024160.

79. Chakravarty, S., Donoghue, J., Waite, A.S., Mahnke, M., Garwood, I.C., Gallo, S., Miller, E.K., and Brown, E.N. (2023). Closed-loop control of anesthetic state in nonhuman primates. PNAS Nexus *2*, pgad293. https://doi.org/10.1093/pnasnexus/pgad293.

80. Brincat, S. (2024). Spynal. Version v0.1.4 (Zenodo). https://doi.org/10.5281/ZENODO.8346151.

81. Herreras, O. (2016). Local Field Potentials: Myths and Misunderstandings. Front. Neural Circuits *10*, 101. https://doi.org/10.3389/fncir.2016.00101.

82. Ahmadi, N., Constandinou, T.G., and Bouganis, C.-S. (2021). Impact of referencing scheme on decoding performance of LFP-based brain-machine interface. J. Neural. Eng. *18*, 016028. https://doi.org/10.1088/1741-2552/abce3c.

83. Shirhatti, V., Borthakur, A., and Ray, S. (2016). Effect of Reference Scheme on Power and Phase of the Local Field Potential. Neural Comput. *28*, 882–913. https://doi.org/10.1162/NECO_a_00827.

84. Thomson, D.J. (1982). Spectrum estimation and harmonic analysis. Proc. IEEE *70*, 1055–1096. https://doi.org/10.1109/PROC.1982.12433.

85. Babadi, B., and Brown, E.N. (2014). A Review of Multitaper Spectral Analysis. IEEE Trans. Biomed. Eng. *61*, 1555–1564. https://doi.org/10.1109/TBME.2014.2311996.

86. Prerau, M.J., Brown, R.E., Bianchi, M.T., Ellenbogen, J.M., and Purdon, P.L. (2017). Sleep Neurophysiological Dynamics Through the Lens of Multitaper Spectral Analysis. Physiology *32*, 60–92. https://doi.org/10.1152/physiol.00062.2015.

STAR★METHODS

KEY RESOURCES TABLE

REAGENT or RESOURCE	SOURCE	IDENTIFIER
Experimental models: Organisms/strains		
Rhesus macaque (Macaca mulatta)	ONPRC (Monkey S), Covance (Monkey P)	RRID: NCBITaxon_9544
Software and algorithms		
Python	Python Software Foundation	RRID: SCR_008394
Spynal	Brincat[80]	https://github.com/sbrincat/spynal
Other		
Utah Array	Blackrock Microsystems	https://blackrockneurotech.com/products/utah-array/

EXPERIMENTAL MODEL AND STUDY PARTICIPANT DETAILS

Experimental design

All surgical and animal care procedures were approved by the Massachusetts Institute of Technology (MIT)'s Committee on Animal Care and were conducted in accordance with the guidelines of the National Institute of Health and MIT's Division of Comparative Medicine. Experiments were performed using two rhesus macaques (Macaca mulatta), referred to as Monkey S and Monkey P. Monkey S was a male, age 11, weighing approximately 10.2 kg, with no previous procedures. Monkey P was a male, age 14, weighing approximately 13.3 kg, who had previously had headpost and chamber insertion procedures. Animals were pair-housed on 12 h day/night cycles and maintained in a temperature-controlled environment (80°F).

Ketamine and dexmedetomidine were administered as an intramuscular bolus to monkeys at sub-anesthetic (1 mg/kg ketamine, 5 μg/kg dexmedetomidine) and anesthetic (10 mg/kg ketamine, 20 μg/kg dexmedetomidine) doses. There were 13 sub-anesthetic dose ketamine sessions (6 with Monkey P, 7 with Monkey S), 16 sub-anesthetic dose dexmedetomidine sessions (8 with Monkey P, 8 with Monkey S), 12 anesthetic dose ketamine sessions (6 with Monkey P, 6 with Monkey S), and 16 anesthetic dose dexmedetomidine sessions (8 with Monkey P, 8 with Monkey S). One anesthetic ketamine session with monkey P was excluded from analysis due to noise from an unknown source. Induction of anesthetic effects was measured by loss of responsiveness in a lever-pressing task. In this task monkeys were trained to press a lever in response to a tone and received a juice reward for a correct response. All monkeys responded regularly before anesthetic injection, then stopped responding to the lever-pressing task before the period from which the "during anesthetic" data was taken for analysis. Changes in spectral LFP power consistent with known effects of ketamine and dexmedetomidine began around 3–4 min after anesthetics were injected and could be seen throughout the period analyzed during anesthetics (Figure S1B), which began 10 min after drug administration.

To study the effects of anesthetics on neural synchrony in PFC, neural activity was recorded continuously throughout the experiment (before, during, and after anesthetic injection) with chronically implanted Utah arrays placed in the left and right ventrolateral PFC and dorsolateral PFC (referred to as L-Ven, R-Ven, L-Dor, and R-Dor). Arrays were placed on either side of the principal sulcus in ventrolateral and dorsolateral PFC. Each array had a regularly spaced grid of 6x6 electrodes, 400 μm apart (minus the four corner locations, for a total of 32 channels per array). All channels were referenced to a wire inserted under the dura in one of the craniotomies.

In periods before and during anesthetics, the monkeys were presented with a separate passive auditory task, in which varying tones were played but monkeys were not required to respond. All analysis was performed on time periods during which the auditory task was happening. Results were indistinguishable during and between blocks of sounds within the auditory task period, so we pooled data across the entire period for analysis.

METHOD DETAILS

LFP processing

LFPs were recorded at 1kHz. For sessions with Monkey P (excluding three anesthetic-dose ketamine sessions), noise was removed at 60, 120, and 180 Hz with online Butterworth notch filtering, resulting in a dip in power around 60 Hz (higher frequencies were not analyzed here). For Monkey S (and the three monkey P sessions), filtering was performed offline, after data collection. We estimated the line noise at the 1st through 8th harmonics of 60 Hz (i.e., 60–480 Hz in steps of 60) by fitting the raw data on each channel with a temporally adaptive sine function at each given frequency. The fitted sinusoids were then subtracted from the data. Due to the effects of the notch filtering, the 60 Hz region is blocked off in further analyses.

To remove common noise and signal from the reference in the LFPs, we used Lepage et al.'s rCAR.[15] Many methods exist for removing noise from LFPs, which each have different benefits and drawbacks[81,82]; we chose this method due to its reduced impact on phase relationships. Methods such as no re-referencing or global mean subtraction can both distort phase relationships between signals. No re-referencing can lead to an increase in phase alignment at the frequency of any common noise or signal inserted by the reference channel. Global mean subtraction can induce spurious phase offsets.[83] rCAR uses a robust maximum-likelihood type estimator to calculate the reference signal, and it is shown to be empirically better at preserving the phase of signals than a global mean reference [15]. We compare these methods in Figure S4, finding slight variation in the phase distributions for each method, but consistent overall trends in the changes in phase relationships during anesthesia.

To identify outlier channels, we calculated the standard deviation of the LFP from each electrode in a session. We then found the interquartile range of standard deviations for all channels in a session, and we removed channels with a standard deviation more than 5 interquartile ranges outside of the overall range, with an average of 3.8 channels out of 128 removed per session.

Spectral analysis

We used multitaper spectral estimation on a series of overlapping time windows to analyze data in the frequency domain. LFPs were split into 1 s time windows, beginning every 0.1 s (so each window had 0.9 s overlap with the next one). We selected 1 s time windows because ketamine anesthesia causes up and down states in which alternating bands of frequency are higher in power, and these states have been found to last about 1 s on the lower end in monkeys.[8] However, we found that the results did not change significantly when using a 2 s time window (Figure S4). We calculated the multitaper spectrogram[84–86] for each window using a time-half bandwidth product of 2 with 3 tapers (as in Garwood et al.[8]) over the frequency range of 1–100 Hz. Analyses were performed using the spynal Python package.[80]

PLV, coherence, phase offset

PLV, coherence, and phase offset were calculated between pairs of channels on indicated arrays. For a comparison between two given arrays, we analyzed all possible pairs of channels between the two arrays. We calculated the cross spectrum C_{XY} by multiplying signal X by the complex conjugate Y^* of signal Y (in the frequency domain) at each time window/taper for each channel pair. We also calculated auto spectra C_{XX} and C_{YY} by multiplying a signal by its own complex conjugate at each time window/taper.

To calculate the PLV, we took the absolute value of the average normalized cross spectrum. To calculate coherence, we divided the cross spectrum of two channels by the square root of the product of each channel's auto spectrum. To calculate the phase offset, we took the angle of the cross spectrum. We then averaged over the tapers, which are independent estimates of the signal. For within-array analyses, we took all possible pairings of channels within an array (excluding self-pairs) and then sorted the pairings by distance between sites.

$$C_{XY} = X(f)\cdot Y^*(f), C_{XX} = X(f)\cdot X^*(f), C_{YY} = Y(f)\cdot Y^*(f)$$

$$PLV_{XY} = |C_{XY}|$$

$$Coh_{XY} = \left|\frac{C_{XY}}{\sqrt{C_{XX}\cdot C_{YY}}}\right|$$

$$\Delta\phi_{XY} = arg(C_{XY})$$

PLV and coherence are dimensionless measures ranging from 0 to 1. Phase offsets range from −180° to 180°. Analyses were performed using the spynal Python package.[80]

Phase histograms

Phase offset histograms show the distribution of phase offsets between all channel pairs in indicated regions, accumulated across all time points within a given recording period (before or during anesthetics). Phase offsets were calculated as indicated above and normalized by the total count of phase values contained in each histogram. The histograms show the distribution over time points and channel pairs (neither time nor channel pairs were averaged out). The histograms have 50 bins, so a uniform distribution across all phase offsets would result in values of 0.02 across all bins. We tested the histograms with finer-grained binning (500 bins) to ensure that no aspects of the distribution were occluded by the choice of bin size and confirmed that they were qualitatively similar. The histograms show phase offsets for the 1–4 Hz frequency range.

Phase alignment index (as in Figure 1D) was calculated by taking the cosine of each phase offset and averaging over time and channel pairs within a session. We chose to take the cosine of the phase offset because the peaks of the phase histograms tended toward 0° and 180°. In this metric, a circular uniform distribution of phases has an average value of zero, while distributions with more weight toward 0° or 180° have positive or negative values, respectively. Note that distributions weighted toward +/−90° would also have a phase alignment index of zero; however, the distributions investigated here were not weighted in those directions. Phase alignment index is a dimensionless measure ranging from −1 to 1.

Instantaneous phase

The instantaneous phase of the example traveling wave in Figure 4 was calculated by forward and reverse bandpass filtering the LFP using a 3rd order Butterworth filter in the 1–4 Hz range, then taking the Hilbert transform and calculating the angle of the signal at the indicated time points.

QUANTIFICATION AND STATISTICAL ANALYSIS

Line plots represent averages across sessions and shaded regions represent 99% confidence intervals on across-session averages. Confidence intervals are nonparametric bootstraps across session means with 100,000 replicates. Stars indicate significant differences between metrics before and during anesthesia at $p < 0.01$ level, calculated with a pairwise permutation test using 100,000 replicates. Bars (in Figures 3A and 3C) indicate significant differences between metrics calculated for low and high doses of anesthetics at $p < 0.01$ level, calculated with a permutation test using 100,000 replicates. p-values were corrected for multiple comparisons across the different frequencies using the Benjamini/Hochberg procedure for controlling the false discovery rate.